JACS
JOURNAL OF THE AMERICAN CHEMICAL SOCIETY
Communication
pubs.acs.org/JACS

Colloidal InSb Nanocrystals

Wenyong Liu,[†] Angela Y. Chang,[‡,§] Richard D. Schaller,[‡,§] and Dmitri V. Talapin*[,†,‡]

[†]Department of Chemistry and James Frank Institute, University of Chicago, Illinois 60637, United States
[‡]Center for Nanoscale Materials, Argonne National Lab, Argonne, Illinois 60439, United States
[§]Department of Chemistry, Northwestern University, Evanston, Illinois 60208, United States

Supporting Information

ABSTRACT: We report the colloidal synthesis of monodisperse nanocrystals (NCs) of InSb, which is an important member of III−V semiconductor family. Colloidal InSb NC quantum dots showed well-resolved excitonic transitions in the near-infrared spectral range, with the optical band gaps tunable from ∼1.03 eV (1200 nm) to ∼0.71 eV (1750 nm) corresponding to 3.3 and 6.5 nm InSb NCs, respectively. We observed size-tunable band edge photoluminescence that could be significantly enhanced by growing InSb/CdSe or InSb/CdS core−shell nanostructures. Films of InSb NCs capped with S^{2-} ions showed ambipolar charge transport.

In electronics and photovoltaics, III−V semiconductors exhibit excellent physical properties that are broadly utilized.[1] In particular, indium antimonide (InSb) is used for infrared detectors and ultrafast electronic circuits because of its direct band gap (0.17 eV at 300 K)[2] and very high carrier mobility. This material has the highest room-temperature electron mobility (∼78 000 $cm^2/(V\ s)$)[2] among all known semiconductors, except maybe recently discovered carbon-based materials. An extremely small effective mass for electrons ($m_e^* = 0.014m_o$, where m_o is the free electron mass) and small effective mass for holes ($m_h^* = 0.25m_o$) result in the largest known value for the Bohr exciton radius of ∼60 nm.[3,4] Bulk InSb also has the smallest exciton binding energy (0.5 meV)[2] among all semiconductors. As a result, reducing the size of InSb crystals down to sub-10 nm range should lead to very strong quantum confinement, at least comparable to that in PbSe, HgTe, and Cd_3As_2, which have Bohr exciton radii of ∼45, ∼40, and ∼47 nm, respectively.[4−6]

InSb quantum wells, nanowires, and quantum dots have been prepared by chemical vapor deposition and molecular beam epitaxy (MBE) techniques.[7,8] At the same time, the colloidal synthesis of III−V nanocrystals (NCs) is rather delicate,[9] and as a result, the chemistry of III−V NCs is less developed compared to other semiconductor NCs. Until now only InP and InAs NCs have been synthesized in the form of monodisperse and well-crystallized NCs, and their optical properties and device applications have been extensively explored.[10−13] It was shown that InAs NCs can be doped with Sb forming $InAs_xSb_{1-x}$ ($x > 0.85$) particles.[14] Numerous attempts have been made to prepare colloidal NCs of other important III−V materials, such as InSb, GaAs, and InN, unfortunately with only modest success.[15] For example, previous work on the colloidal synthesis of InSb nanoparticles[16] had not reported conclusive data on the formation of InSb NCs, such as X-ray diffraction or high-resolution electron microscopy. We report on the colloidal synthesis of InSb NCs and present their size-dependent optical and electronic properties.

We synthesized InSb NCs by reacting $InCl_3$ and $Sb[N(Si(Me)_3)_2]_3$ in oleylamine in the presence of lithium triethylborohydride ($LiEt_3BH$), also known as superhydride. $Sb[N(Si(Me)_3)_2]_3$ was prepared as described in the Supporting Information (SI) and its purity was verified by ^{13}C and H NMR (Figure S1). In a typical synthesis, 5 mL of 2.0 M $LiEt_3BH$ solution in dioctyl ether was loaded into a three-neck flask filled with 12 mL of anhydrous degassed oleylamine at room temperature, immediately followed by the injection of a premixed solution containing 0.8 mmol of $InCl_3$ and 0.8 mmol of $Sb[N(Si(Me)_3)_2]_3$ in 3.2 mL of *n*-trioctylphosphine and 0.5 mL of toluene. Upon addition, the reaction mixture turned brown and then black. At this stage, the reaction temperature was increased to 260 °C at the rate of about 3 °C/min. The solution was annealed at 260 °C for 20 min and cooled down to the room temperature. Five mL of oleic acid (OA) were added to the crude solution to neutralize excessive superhydride and attach oleate ligands to the NC surface. Then, crude solution was centrifuged to separate insoluble byproducts from the NCs which remained in supernatant.

We found that the presence of $LiEt_3BH$ was crucial for the formation of InSb NCs. In the absence of superhydride, $InCl_3$, and $Sb[N(Si(Me)_3)_2]_3$ did not react below 200 °C. At higher temperatures these precursors formed a black amorphous precipitate. Control experiments showed that mixing $LiEt_3BH$ with $InCl_3$ in oleylamine resulted in the formation of metallic indium and mixing $LiEt_3BH$ with $Sb[N(Si(Me)_3)_2]_3$ generated black amorphous product presumably containing antimony clusters.[17] We therefore propose that the role of superhydride is to activate the indium and antimony precursors through the formation of highly reactive $In^{(0)}$ and $Sb^{(0)}$ intermediates. Further mechanistic studies will be necessary to test this hypothesis and elucidate the microscopic reaction pathway. Interestingly, traditional metalorganic chemical vapor deposition (MOCVD) synthesis of III−V semiconductors typically requires the presence of H_2 at high temperatures, indicating the importance of a reductive environment for growing crystalline III−V materials.[18,19]

Received: October 4, 2012
Published: December 2, 2012

 © 2012 American Chemical Society dx.doi.org/10.1021/ja309821j | J. Am. Chem. Soc. 2012, 134, 20258−20261

The average size of as-synthesized InSb NCs can be tuned by changing the growth temperature and the amount of $LiEt_3BH$. Higher temperature and longer annealing times generally yielded larger NCs. InSb NCs with sizes ranging from 4.5 to 7 nm were obtained after growth at temperatures between 240 and 260 °C for 20 min using a molar ratio of 1:12.5 $InCl_3$ to $LiEt_3BH$, corresponding to a 2-fold excess with respect to the quantity needed for complete reduction of indium and antimony precursors. When the $InCl_3$ to $LiEt_3BH$ molar ratio was reduced to 1:6.25, 3.4−4.5 nm InSb NCs were obtained at 240 °C annealing temperature. InSb NCs prepared below 240 °C often showed poor crystallinity.

As-synthesized InSb NCs showed ∼15% size distribution (Figure S2). To improve the size distribution of InSb NCs, we applied size-selective precipitation using toluene and acetonitrile as the solvent and nonsolvent, respectively. A similar approach was used for obtaining monodisperse InP and InAs NCs.[11,12] After size selection, the monodisperse InSb NCs were isolated and redispersed in toluene, hexane, or tetrachloroethylene (TCE).

Figure 1a,b shows typical TEM images of InSb NCs with the average size of 4.2 and 6.3 nm, respectively. The high-resolution

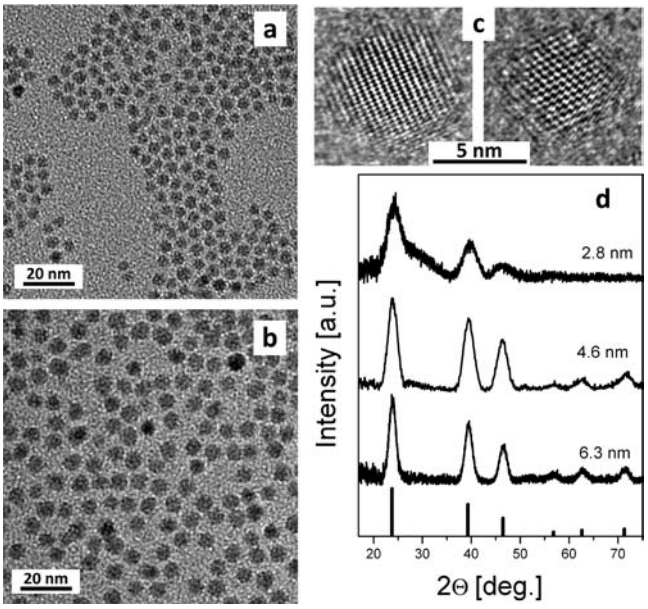

Figure 1. (a,b) TEM images of 4.2 and 6.3 nm InSb NCs. (c) High-resolution TEM images of InSb NCs viewed along different zone axes. (d) Powder X-ray diffraction patterns of InSb NCs with various sizes. Sizes above each curve are derived from the Scherrer equation, applied to the fwhm of the (111) reflection. The vertical lines on the bottom are the corresponding positions and intensities of X-ray reflections for bulk InSb.

images shown in Figure 1c demonstrate highly crystalline nanoparticles. The powder X-ray diffraction patterns shown in Figure 1d revealed cubic zinc blende crystal structure of InSb NCs, identical to that of bulk InSb. The NC sizes calculated from the width of diffraction peaks using Scherrer's equation were consistent with the NC size in TEM images, further proving good crystallinity of the InSb NCs. When exposed to air, small InSb NCs showed partial oxidation, and the formation of indium and antimony oxides was observed in powder XRD patterns (Figure S3). Elemental analysis of synthesized InSb NCs by ICP-OES showed a small excess of antimony, with an In:Sb molar ratio of about 1:1.13.

Colloidal solutions of InSb NCs showed size-dependent absorption spectra with characteristic peaks in the near-infrared corresponding to the optical transitions between the excitonic states (Figure 2a). The spectral positions of the absorption

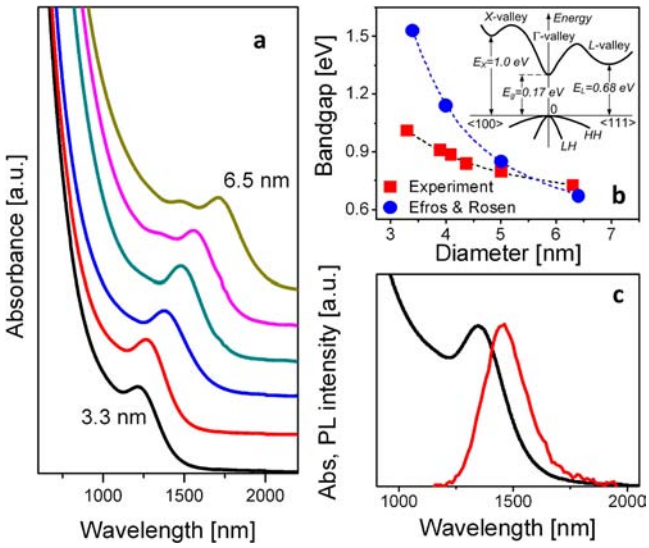

Figure 2. (a) Absorption spectra of InSb NCs in TCE with sizes between 3.3 and 6.5 nm. (b) Size-dependence of the optical band gap measured for InSb NCs at room temperature compared to the calculations by Efros and Rosen (ref 20). Inset shows the band diagram of bulk InSb at 300K. HH and LH indicate the heavy and light holes, respectively. (c) Typical absorption (black) and photoluminescence (red) spectra for size-selected InSb NCs in TCE.

peaks depended strongly on the NC diameter, as expected for quantum confined NCs. The optical band gap of InSb NCs, measured as the energy of the lowest excitonic transition, could be tuned from ∼1200 nm (1.03 eV) for 3.3 nm NCs to 1750 nm (0.71 eV) for 6.5 nm NCs (Figure 2b). Taking into account small electron and hole effective masses, one might expect larger confinement energy for this size range. For example, simple parabolic band model[21] predicts a 4.6 eV bandgap for 5 nm InSb NCs, which is in obvious disagreement with the experimental data. Efros and Rosen (ER) calculated size dependence for quantum state levels in InSb NCs using an eight-band Pidgeon and Brown model which accounted for the coupling between conduction and valence bands.[20] We compared predicted $1S_{3/2}(h) - 1S_{1/2}(e)$ transition energies (calculated as the difference between electron and hole energies reduced by the Coulombic term, $1.8e^2/\varepsilon R$, where ε is the dielectric constant and R is the NC radius) with experimental data and found that ER calculations provided rather accurate predictions for the NCs sizes above ∼5 nm (Figure 2b) but overestimated the band gaps for smaller InSb NCs. There can be various reasons why theoretical transition energies are systematically higher than experimental ones, such as underestimated leakage of the wave functions into the surrounding medium.[22] Here we also want to point out the presence of energetically closely spaced valleys in the conduction band of InSb and some other III−V semiconductors. In bulk InSb, the bottom of the L-valley is only 0.51 eV above the bottom of the Γ-valley (Figure 2b, inset). Because the electron effective mass in the Γ-valley ($m_\Gamma^* = 0.014m_0$) is ∼18 times smaller than that

dx.doi.org/10.1021/ja309821j | J. Am. Chem. Soc. 2012, 134, 20258−20261

in the L-valley ($m_L^* = 0.25m_0$), the electrons in the Γ-valley should be more responsive to the quantum confinement than in the L-valley. As a result, the energy difference between the lowest quantum confined states in Γ- and L-valleys is expected to decrease with decreasing NC size, and at a certain size, we may expect even a transition from direct to indirect band structure of InSb NCs. Conventional theoretical models typically ignore the band structure beyond the Γ-valley which can lead to qualitatively wrong descriptions of strongly quantum confined III−V quantum dots. Only recently has the possibility of direct-to-indirect transition been studied theoretically for GaAs quantum dots.[23]

Our experimental data suggest that InSb NCs retain the direct gap character of the bulk material, at least for sizes >3.6 nm. Figure 2c shows an example of the photoluminescence (PL) spectrum of 3.8 nm InSb NCs. The observation of the band-edge luminescence suggests that 3.8 nm InSb NCs preserve their direct band gap electronic structure. The PL efficiency was rather weak at room temperature (below 1%) and significantly increased at low temperatures.

We noticed significant sample-to-sample variations in the PL efficiency of InSb NCs, which is rather common for colloidal NCs. Generally, the stability and PL efficiency of semiconductor NCs can be improved by growing a wide-gap shell of another semiconductor.[24] The zinc blende crystal structure of InSb NCs makes them compatible with II−VI materials. On the other hand, the large lattice constant (a = 6.479 Å) of InSb should create a large interfacial strain with many II−VI and III−V shells, with the exception of CdTe (a = 6.482 Å) that forms a nearly strain-free interface with InSb. It was noticed in the MBE studies that at elevated temperatures, InSb surface can react with Te, forming In_2Te_3 and Sb.[25] In MBE this problem can be avoided by using excess Cd precursor.[25] Our preliminary studies revealed that a crystalline CdTe shell can be grown around InSb NCs, resulting in some improvement of the PL efficiency (Figure S4). However, it also resulted in a small blue shift of the absorption peak (Figure S5),[26] which suggested either partial alloying or etching of InSb cores before or during the growth of CdTe shell. A similar effect was observed when we attempted to grow a ZnTe shell.[26] So far the best results have been achieved for CdSe and CdS as the shell materials. In a typical preparation of InSb/CdS core−shell NCs, the InSb cores were overcoated with CdS shells at 60 °C in oleylamine using $Cd(Me)_2$ and bis(trimethysilyl)sulfide as Cd and S precursors, respectively.[26] In both InSb/CdSe and InSb/CdS cases we observed the formation of core−shell NCs, despite ~6.6% and 10.0% lattice mismatch between InSb and CdSe or CdS phases, respectively. Figures 3a, S6, and S7 show the TEM images and X-ray diffraction patterns of corresponding InSb cores and InSb/CdS core−shells. Upon the growth of CdS shell, the NC shape evolved from near-spherical to partially tetrahedrally faceted. An average increase in NC size by 0.6 nm was consistent with the formation of about one monolayer thick CdS shell. The formation of CdSe and CdS shells resulted in the red shifts of the absorption maxima of InSb NCs (Figures 3b and S5), which can be explained by partial leakage of the wave functions into the shell material. We also observed significant improvement of the PL efficiency. For example, InSb/CdS NCs shown in Figure 3a showed ~200-fold increase of the PL efficiency compared to original InSb cores (Figure 3c). The PL decay trace shown in Figure 3d could be fitted with the fast component, presumably corresponding to some nonradiative recombination channel, followed by a slow nearly

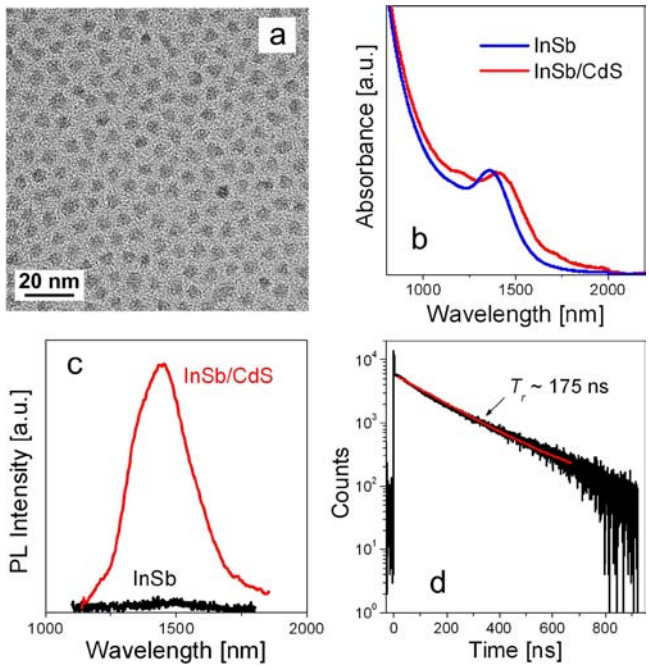

Figure 3. (a) TEM image of InSb/CdS core−shells. (b) Absorption spectra of InSb cores and InSb/CdS core−shells. (c) PL spectra of InSb core and InSb/CdS core−shell NCs measured under identical conditions. (d) Time-resolved PL decay for InSb/CdS core−shell NCs excited with 40 ps pulses at 705 nm.

monoexponential component with ~175 ns decay time that likely corresponded to the radiative lifetime (T_r). The component with similar lifetime (~160 ns) was also observed in the PL decay of bare InSb NCs (Figure S8). This lifetime is much shorter than T_r of lead chalcogenide NCs[27] which makes InSb NCs potentially interesting material for near- and mid-IR emission applications.

We also carried out preliminary studies of the surface chemistry of InSb NCs and charge transport in the InSb NC films. It is well-known that surface ligands with long hydrocarbon chains, such as oleic acid or oleylamine, negatively affect the electronic transport in NC-based devices.[28] To improve the conductivity of InSb NC solids, we replaced the oleate ligands with S^{2-} or Te^{2-} ligands. For this purpose we performed the phase transfer of organics-capped InSb NCs from toluene into highly polar N-methyl formamide (NMF) using K_2S or K_2Te.[29,30] No etching of the NC surface was observed during the ligand exchange at the room temperature (Figure S9). To study doping and transport in the films made of InSb/S^{2-}/K^+ NCs, we followed standard NC FET fabrication steps.[26] Figure S10 shows the output and transfer characteristics of InSb NC FETs made of S^{2-}-capped 4.5 nm InSb NCs. We observed the ambipolar charge transport with electron and hole mobilities 1.5×10^{-4} and 6×10^{-4} cm^2/(V s), respectively. These preliminary data show that InSb NCs electronically behave as a typical narrow gap semiconductor.

In conclusion, we reported the first colloidal synthesis of monodisperse and well crystallized sub-10 nm InSb NCs. InSb NCs showed size-dependent absorption and PL spectra as well as other characteristic properties of direct gap semiconductor NCs. The stability and PL efficiency of InSb NCs could be significantly improved by growing core−shell InSb/CdSe and InSb/CdS nanoheterostructures. InSb NCs can be used in field-effect devices and show ambipolar charge transport. There is

dx.doi.org/10.1021/ja309821j | J. Am. Chem. Soc. 2012, 134, 20258−20261

more room for further optimization of InSb-based core−shell nanostructures and devices. These new NCs can find important applications, e.g., in near- or mid-IR emitters and detectors. Another interesting feature of InSb is its low melting point compared to other semiconductors (T_m = 527 °C). One can think of using InSb NCs as soluble precursors for deposition of InSb films, e.g., by spin coating the NC colloids followed by rapid annealing at near-T_m temperatures.

■ ASSOCIATED CONTENT

Supporting Information

Additional experimental details and figures. This material is available free of charge via the Internet at http://pubs.acs.org.

■ AUTHOR INFORMATION

Corresponding Author

dvtalapin@uchicago.edu

Notes

The authors declare no competing financial interest.

■ ACKNOWLEDGMENTS

We thank J.-S. Lee for the FET measurements and C. Jiang for ICP-OES measurements. The work on synthesis of NCs was supported by Camille Dreyfus Teacher-Scholar Awards Program and NSF CAREER under award no. DMR-0847535. The work was also partially supported by the University of Chicago and the Department of Energy under Department of Energy contract no. DE-AC02-06CH11357 awarded to UChicago Argonne, LLC, operator of Argonne National Laboratory. D.V.T. thanks the David and Lucile Packard Foundation for their generous support. This work was performed, in part, at the Center for Nanoscale Materials, a U.S. Department of Energy, Office of Science, Office of Basic Energy Sciences User Facility under Contract No. DE-AC02-06CH11357. This work also used facilities supported by NSF MRSEC Program under award no. DMR-0213745.

■ REFERENCES

(1) Adachi, S., *Properties of Group-IV, III-V and II-VI Semiconductors*; Blackwell Science: Oxford, 2005; p 387.

(2) Group IV, Elements, IV-IV and III-V Compounds. Part b - Electronic, Transport, Optical and Other Properties. In *Landolt-Börnstein - Group III Condensed Matter*, Madelung, O.; Rössler, U.; Schulz, M., Eds.; Springer-Verlag: Germany, 2002; Vol. *41A1b*.

(3) Wise, F. W. *Acc. Chem. Res.* **2000**, *33*, 773−780.

(4) Yoffe, A. D. *Adv. Phys.* **1993**, *42*, 173.

(5) Keuleyan, S.; Lhuillier, E.; Guyot-Sionnest, P. *J. Am. Chem. Soc.* **2011**, *133*, 16422−16424.

(6) Harris, D. K.; Allen, P. M.; Han, H.-S.; Walker, B. J.; Lee, J.; Bawendi, M. G. *J. Am. Chem. Soc.* **2011**, *133*, 4676−4679.

(7) Bennett, B. R.; Magno, R.; Shanabrook, B. V. *Appl. Phys. Lett.* **1996**, *68*, 505−507.

(8) Mingo, N. *Appl. Phys. Lett.* **2004**, *84*, 2652−2654.

(9) Nozik, A. J.; Micic, O. I. *MRS Bull.* **1998**, *23*, 24−30.

(10) Tessler, N.; Medvedev, V.; Kazes, M.; Kan, S.; Banin, U. *Science* **2002**, *295*, 1506−1508.

(11) Micic, O. I.; Curtis, C. J.; Jones, K. M.; Sprague, J. R.; Nozik, A. J. *J. Phys. Chem.* **1994**, *98*, 4966−4969.

(12) Guzelian, A. A.; Banin, U.; Kadanich, A. V.; Peng, X.; Alivisatos, A. P. *Appl. Phys. Lett.* **1996**, *69*, 1462−1464.

(13) Battaglia, D.; Peng, X. *Nano Lett.* **2002**, *2*, 1027−1030.

(14) Kim, S.-W.; S, S.; Lee, B. Y. *Chem. Comm* **2006**, 4811−4813.

(15) Chen, Z.; Li, Y.; Cao, C.; Zhao, S.; Fathololoumi, S.; Mi, Z.; Xu, X. *J. Am. Chem. Soc.* **2012**, *134*, 780−783.

(16) Evans, C. M.; Castro, S. L.; Worman, J. J.; Raffaelle, R. P. *Chem. Mater.* **2008**, *20*, 5727−5730.

(17) Antimony is known for its rich cluster chemistry that includes relatively stable Sb_3^{3-} and Sb_7^{3-} zintl ions, see: Corbett, J. D. *Chem. Rev.* **1985**, *85*, 383−397]..

(18) Hoang, A. M.; Chen, G.; Haddadi, A.; Pour, S. A.; Razeghi, M. *Appl. Phys. Lett.* **2012**, *100*, 211101.

(19) Yoon, J.; Jo, S.; Chun, I. S.; Jung, I.; Kim, H.-S.; Meitl, M.; Menard, E.; Li, X.; Coleman, J. J.; Paik, U.; Rogers, J. A. *Nature* **2010**, *465*, 329−333.

(20) Efros, A. L.; Rosen, M. *Phys. Rev. B* **1998**, *58*, 7120−7135.

(21) Brus, L. *J. Phys. Chem.* **1986**, *90*, 2555−2560.

(22) Banin, U.; Lee, C. J.; Guzelian, A. A.; Kadavanich, A. V.; Alivisatos, A. P.; Jaskolski, W.; Bryant, G. W.; Al, L. E.; Rosen, M. *J. Chem. Phys.* **1998**, *109*, 2306−2309.

(23) Luo, J.-W.; Franceschetti, A.; Zunger, A. *Phys. Rev. B* **2008**, *78*, 035306.

(24) Reiss, P.; Protière, M.; Li, L. *Small* **2009**, *5*, 154−168.

(25) Zahn, D. R. T.; Williams, R. H.; Golding, T. D.; Dinan, J. H.; Mackey, K. J.; Geurts, J.; Richter, W. *Appl. Phys. Lett.* **1988**, *53*, 2409−2410.

(26) Additional details in SI.

(27) Kovalenko, M. V.; Schaller, R. D.; Jarzab, D.; Loi, M. A.; Talapin, D. V. *J. Am. Chem. Soc.* **2012**, *134*, 2457−2460.

(28) Talapin, D. V.; Lee, J.-S.; Kovalenko, M. V.; Shevchenko, E. V. *Chem. Rev.* **2010**, *110*, 389−458.

(29) Nag, A.; Kovalenko, M. V.; Lee, J.-S.; Liu, W.; Spokoyny, B.; Talapin, D. V. *J. Am. Chem. Soc.* **2011**, *133*, 10612−10620.

(30) Kovalenko, M. V.; Scheele, M.; Talapin, D. V. *Science* **2009**, *324*, 1417−1420.